Aerospace Science and Technology 73 (2018) 164–172

Contents lists available at ScienceDirect

Aerospace Science and Technology

www.elsevier.com/locate/aescte

An experimental study of surface wettability effects on dynamic ice accretion process over an UAS propeller model

Yang Liu, Linkai Li, Haixing Li, Hui Hu *

Department of Aerospace Engineering, Iowa State University, 2271 Howe Hall, Room 1200, Ames, IA 50011, USA

ARTICLE INFO

Article history:
Received 25 September 2017
Received in revised form 1 December 2017
Accepted 2 December 2017
Available online 6 December 2017

Keywords:
Ice accretion
Surface water transport
Surface wettability
Latent heat release
Unmanned Aerial System

ABSTRACT

An experimental study was conducted to evaluate the effects of surface wettability on the dynamic ice accretion process over the surface of a rotating Unmanned-Aerial-System (UAS) propeller model and the resultant aerodynamic performance degradation due to the ice accretion. A propeller model was installed in an Icing Research Tunnel at Iowa State University (i.e., ISU-IRT) with its surface wettability changed significantly (i.e., hydrophilic surface *versus* superhydrophobic surface). In addition to acquiring "phase-locked" images to reveal the dynamic ice accretion process over the rotating propeller surface, the thrust generation and the required power input to drive the propeller model to operate at a constant rotation speed were also measured during the ice accretion process. The dynamic ice accretion process over the rotating propeller surface was found to vary remarkably with changes to the propeller surface wettability. By making the propeller surface superhydrophobic, the detrimental effects of the ice accretion on the aerodynamic performance of the propeller model were found to be mitigated greatly with much less ice accretion over the propeller surface, significant reduction of the thrust loss and less demand for extra power consumption due to the ice accretion, in comparison with the case with the propeller surface being hydrophilic.

1. Introduction

Inflight icing has been found to pose significant safety and performance concerns for both unmanned and manned aircraft in a cold climate [1]. With the rapid development of Unmanned Aerial Systems (i.e., UAS in short) in recent years, UAS icing has become an urgent-to-solve problem in order to ensure safe and efficient operation of UAS in cold weather [2]. In comparison with conventional, large-sized manned aircraft, a lightweight UAS is more susceptible to inflight icing problems due to the lower cruising altitude with relatively higher liquid water content (*LWC*) levels and warmer air temperatures, smaller excess power margin to offset the increased drag caused by ice accretion [3], lower flight velocity resulting in longer exposure to icing conditions, and more damage to important sensors onboard [4]. The potential damage of inflight icing to UAS renders their operation unfeasible in cold weather. As described in Botura and Fahrner [5], 25% of UAS flights had encountered ice during a specific military action that have negatively impacted the success of the mission. The common icing avoidance strategies for UAS in nowadays are keeping UAS on the ground [6] or modifying path planning [7]. This would greatly reduce the operation capability of UAS in cold climate. This is particularly troubling for military UAS applications, in which icing conditions can lead to aborted missions and the loss of crucial tactical capabilities.

To mitigate the detrimental effects of ice accretion on the operational performance of aircraft (for both unmanned and manned), various anti-/de-icing techniques have been developed and employed to prevent or reduce ice accretion on the aircraft. While anti-icing refers to the prevention of any buildup of ice on a surface, de-icing denotes the case where ice has already formed on a surface, which is subsequently removed. Most of the anti-/de-icing methods currently used for UAS icing mitigation can be classified in two categories: active and passive methods. While active methods rely on an external system, passive methods take advantage of the physical properties of wing or/and propeller surfaces to eliminate or prevent ice formation and accretion. Most of the active systems developed for UAS icing mitigation are thermal systems that remove ice buildup by applying heat to iced wings [8–12]. It should be noted that, massive heating for de-icing operation would not be applicable to UAS due to the limited payload and scant excess power. Furthermore, caution must be taken in the design of thermal systems since runback water can re-freeze after passing the heated area. In the present study, we pay special attention to

* Corresponding author.
E-mail address: huhui@iastate.edu (H. Hu).

https://doi.org/10.1016/j.ast.2017.12.003
1270-9638/

passive methods which take advantage of surface properties (e.g., wettability) of UAS airframes to prevent or eliminate ice formation and accretion without additional power input.

Inspired by the outstanding self-cleaning capability of lotus leaves and duck feathers, a number of studies have been conducted in recent years to develop coatings to make superhydrophobic surfaces [13–15], on which water droplets bead up with a very large contact angle (i.e., $>150°$) and drip off rapidly when the surface is slightly inclined (i.e., very small contact angle hysteresis). Such superhydrophobic surfaces have been demonstrated to have the capability of repelling water drops on the surface [9,16–19], delaying the crystallization of water drops that contact the surface [20–22], and reducing the adhesion of aqueous media in both liquid and crystalline states to the surfaces [23–26]. However, the direct correlation between superhydrophobicity and icephobicity has been under debate for several years [27–30]. As described in Hejazi et al. [28], the parallelism between the hydrophobicity and icephobicity suggests a reasonable anti-icing performance of superhydrophobic surfaces (i.e., low adhesion strength and delayed ice crystallization and droplets bouncing). Yet a multifaceted evaluation of freezing delay and liquid-shedding ability and their competing effects were suggested to be taken into account when choosing a superhydrophobic coating as anti-icing surface [27]. It should also be noted that, while most of previous studies on superhydrophobic coatings were accomplished with only simple and static tests (i.e., by spraying water droplets or pouring water onto substrates and then freezing the test samples in refrigerators) to demonstrate their water- and ice-phobic characteristics [31,32], very little can be found in the literature to evaluate their capabilities to suppress "*impact icing*", which is the process pertinent to UAS in-flight icing phenomena. Here, "*impact icing*" is defined as ice formed due to the dynamic collision of super-cooled water droplets onto a surface at a high impact velocity. The structure of impact ice accretion can vary considerably depending upon the conditions in which the ice is formed. Air temperature, air speed, water droplet size, liquid water content, and airframe geometry would all affect the accreted ice structures. Very recently, Waldman et al. [33] conducted an experimental study to demonstrate the feasibility to use a superhydrophobic coating to mitigate impact icing over an airfoil/wing model with the speed of the incoming airflow along with the impinging supper-cooled water droplets being as high as 50 m/s. The aerodynamic stresses from the airflow over the wing surface were found to sweep away impinged water droplets/films from most of the superhydrophobic wing surface to prevent impact ice accretion. However, ice was still found to form near the leading edge of the super-hydrophobic wing in the vicinity of the stagnation line, which highlights one of the major challenges facing hydro- and ice-phobic coating strategies, i.e. when a water droplet impacts a superhydrophobic surface at extremely high velocity, it can penetrate into the surface texture and adopts the Wenzel state, which leads to increased contact area between water and solid surface [34–36] and consequently leads to higher ice adhesion strength. It also illustrates that superhydrophobic coatings that are effectively ice-phobic at nominal conditions may not perform well under impact icing conditions pertinent to inflight icing phenomena.

Unlike most large manned aircraft using turbofan or turbojet engines for propulsion, almost all the UAS are powered by propellers. Since ice may accumulate on every exposed frontal surfaces of UAS, not only on wings, but also on the surfaces of rotating propellers, which can significantly degrade the aerodynamic performance of the propellers. In moderate to severe conditions, the propellers can become so iced up that continued flight would become impossible. In comparison to ice accretion on stationary surfaces, the ice accretion process over rotating propeller surfaces is even more complicated, due to the combined effects of aerodynamics shear forces exerted by the incoming airflow and the centrifugal forces induced by rotation. Furthermore, as revealed in the recent experimental study of Liu et al. [3], ice structures accreted over the rotating propeller blades would be shed off when the centrifugal forces acting on the accreted ice overcome the interfacial adhesion forces between the accreted ice layer and the blade surfaces. By applying a superhydrophobic coating onto propeller blades, the adhesion strength between the accreted ice layers and the blade surfaces can be potentially reduced, as suggested by Wang et al. [37]. Thus, an improved anti-/de-icing performance of the superhydrophobic surface coatings would be expected when applied onto rotating UAS propellers, in comparison with the case over the fixed wing models.

With this in mind, we conducted an experimental study to evaluate the effects of surface wettability on the dynamic ice accretion process over the surface of a rotating UAS propeller model and the resultant performance degradation due to the ice accretion. The experimental study was performed in an Icing Research Tunnel available at Iowa State University (ISU-IRT) with a scaled UAS propeller model operated under a typical glaze icing condition. During the experiment, the surface of the UAS propeller model was treated to change its surface wettability (i.e., hydrophilic surface case *versus* superhydrophobic surface case). The "phase-locked" images were acquired using a high-speed imaging system to reveal the time-evolution of the dynamic ice accretion processes over the surfaces of the rotating propeller with significant changes in surface wettability (i.e., hydrophilic case *vs.* superhydrophobic case). In addition, the aerodynamic performance degradations (i.e., thrust loss and extra power consumption) of the UAS propeller model due to the ice accretion were also assessed to provide more insights into the potential benefits of using superhydrophobic surfaces for UAS in-flight icing mitigation.

2. Experimental setup and test model

2.1. Tested propeller model

Fig. 1 shows the schematic of the UAS propeller model used in the present study, which is a three-blade propeller with a coniptical spinner of 33 mm in diameter in the center of the propeller. As shown schematically in Fig. 1, with their radius being 100 mm (i.e., $R = 100$ mm), the rotor blades of the propeller model have typical airfoil cross sections and platform profiles commonly used in modern UAS propellers. Two airfoil profiles (i.e., ARA-D 13% and ARA-D 20%) were used at different spanwise locations along the rotor blades: while an ARA-D 20% airfoil profile was used between $0.10R$ and $0.30R$, an ARA-D 13% airfoil was used from $0.30R$ through the blade tip. With the prescribed blade platform profiles and twist angles (i.e., optimized based on the freestream airflow velocity and rotational speed of the propeller), a spline function was used to interpolate the prescribed cross section profiles to generate the three-dimensional geometry of the propeller blade using SolidWorks software. While the primary design parameters of the UAS propeller model are listed in Table 1, further details about the dimensions and design of the UAS propeller model can be found in Liu et al. [3].

The propeller model is made of a hard plastic material (i.e., VeroWhitePlus, RGD835 by Stratasys, Inc.), and was manufactured using a rapid prototyping machine (i.e., 3D printer). During the experiments, an aluminum tube with a streamlined cross section was used to support the propeller model when installed in ISU-IRT.

2.2. Surface treatment

In the present study, the surface of the propeller model was treated to be in significantly different wettability (i.e., hydrophilic

Table 1
The design parameters of the UAS propeller model.

Parameter	R (mm)	H (mm)	d_{mount} (mm)	$d_{support}$ (mm)	$a1$ (mm)	$a2$ (mm)	a (mm)
Dimension	100.00	196.10	32.20	30.00	100.96	41.00	146.86

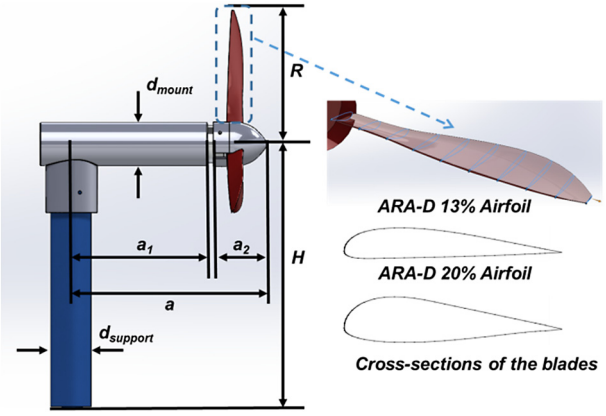

Fig. 1. Schematic of the UAS propeller model used in the present study.

surface case *vs.* superhydrophobic surface case) in order to evaluate the effects of surface wettability on the dynamic ice accretion process over the rotating UAS propeller and the resultant aerodynamic performance degradation due to the ice accretion. For the first test case (i.e., hydrophilic Surface-I case), the surface of the propeller model was coated with several layers of spray-on sandable primer. The primed surfaces were then wet-sanded using a series of progressively finer sandpapers (up to 2000 grit) to achieve a very smooth, glossy finish with a characteristic roughness over the propeller surface being about 25 μm. Then, a readily available all-weather protective spray-on enamel (Rustoleum, Flat Protective Enamel, white in color) was coated onto the primed surface. The sanded primer layers would provide a strong adhesion of the enamel onto the propeller surface. The surfaces (both on the spinner cone and the blades) treated in such an approach has been found to be hydrophilic, as reported in Waldman et al. [33]. For the second test case (i.e., the superhydrophobic Surface-II case), the surface of the propeller model was treated with a spray-on superhydrophobic coating (i.e., Hydrobead Standard and Hydrobead Enhancer, Hydrobead™, San Diego, California USA). While the Hydrobead™ coating is translucent, it can be easily applied onto the top of the Rustoleum enamel base coating. As described in Sun et al. [38], the superhydrophobic Hydrobead™ coating consists of a single-step spray-on base coating to provide a superhydrophobic base layer, and an optional spray-on top coat that further increases the hydrophobicity. In the present study, both the Standard and Enhancer coatings were applied over the surface of the propeller model (both on the spinner cone and the blades). Further information about the wettability characteristics of the two test surfaces will be provided in the "measurement results and discussions" section of the present study.

2.3. Experimental setup

The experimental study was performed in an Icing Research Tunnel available at Aerospace Engineering Department of Iowa State University (i.e., ISU-IRT). The ISU-IRT has a test section of 2.0 m in length × 0.4 m in width × 0.4 m in height with four optically-transparent side walls. It has the capacity to generate a maximum wind speed of 60 m/s and an airflow temperature down to −25 °C. An array of 8 pneumatic atomizer/spray nozzles are installed at the entrance of the contraction section of ISU-IRT to inject micro-sized water droplets (10 ∼ 100 μm in size), which can be sufficiently cooled down to the air temperature during the flight along with the airflow before impacting on the model. By manipulating the water flow rate through the spray nozzles, the liquid water content (*LWC*) in ISU-IRT could be adjusted in the range from $LWC = 0.1$ g/m^3 to 5.0 g/m^3. In summary, ISU-IRT can be used to simulate atmospheric icing phenomena over a range of icing conditions (i.e., from dry *rime* to extremely wet *glaze* ice conditions). Further information about ISU-IRT is available in Waldman and Hu [39].

Fig. 2 shows the schematic of the experimental setup used in the present study. During the ice accretion experiments, the rotor blades of the propeller model were driven using a brushless motor (DJI 2212, 940 KV), which was powered by a direct current (DC) power supply (VOLTEQ HY3050EX). The rotational speed of the model propeller was kept at a constant rotation speed of $n = 3{,}000$ rpm using a digital speed controller/manipulator to adjust the signal duty cycle of the brushless motor. A proportional-integral-derivative (PID) algorithm (i.e., a control loop feedback mechanism) was integrated into the rotation speed control system to achieve automatic rotational speed correction for the propeller model as a disturbance occurs (e.g., ice accretion or ice shedding). The rotational speed of the propeller rotor was also monitored using a digital tachometer (MONARCH PLT200), which would generate a pulsed signal for each rotation cycle of the propeller model. The pulsed-signal generated by the digital tachometer was sent to a digital delay/pulse generator (BNC Model-577) to trigger a high-resolution imaging system (i.e., PCO Tech, PCO-Dimax S4, up to 1279 frames per second @ 2016 pixel by 2016 pixel) along with a 50 mm Macro-lens (Nikon, 50 mm Nikkor 1.8D) to acquire "phase-locked" images to reveal the time evolution of the dynamic ice accretion process over the surface of the rotating propeller model. Two units of 100 W Studio-LED light (RPS Studio Light, Model RS-5610 and RS-5620) were used to provide low-flicker illumination for the image acquisition.

In the present study, the streamline-shaped supporting tube of the propeller model was connected to a high-sensitivity force-moment sensor (JR3 load cell, model 30E12A-I40) to measure the thrust forces generated by the model propeller. The JR3 load cell, which is composed of foil strain gage bridges, is capable of achieving time-resolved measurements of forces and the moments (torques) about each axis. The precision of the JR3 load cell for force measurements is ±0.25% of the full range (40 N). During the experiments, the thrust force data were sampled at a rate of 5,000 Hz for each test case. During the experiment, the electric currents and voltages of the DC power supply applied to the brushless motor were also recorded via a data acquisition system (NI USB-6218). The recorded data were then used to determine the required power inputs to drive the propeller model to rotate at the constant rotation speed of $n = 3{,}000$ rpm during the ice accretion experiment.

3. Measurement results and discussion

3.1. Characteristics of the two compared propeller surfaces with significantly different wettability

As described above, the two different kinds of propeller surfaces with significant differences in surface wettability (i.e., hydrophilic Surface-I *vs.* superhydrophobic Surface-II) were prepared for the present study. The contact angles of sessile water droplets

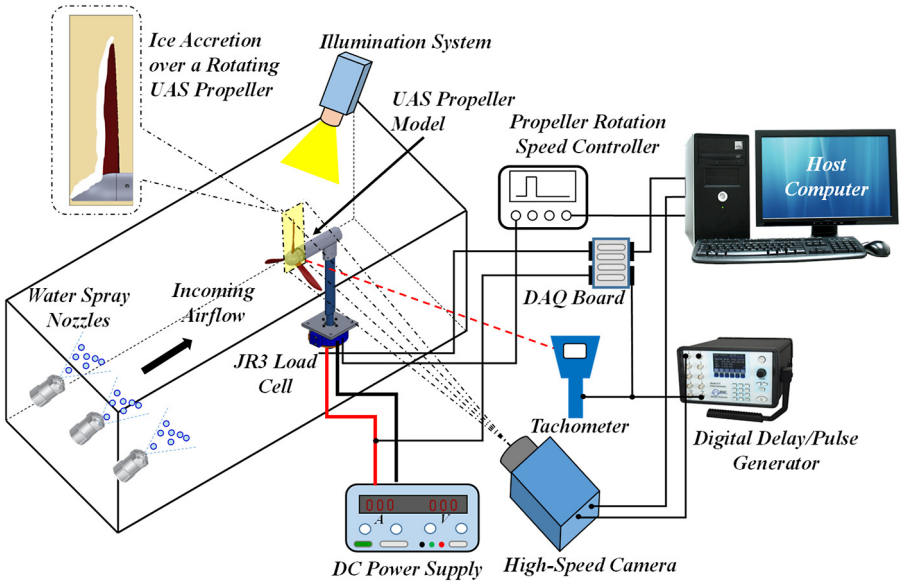

Fig. 2. The schematic of the experimental setup used in the present study.

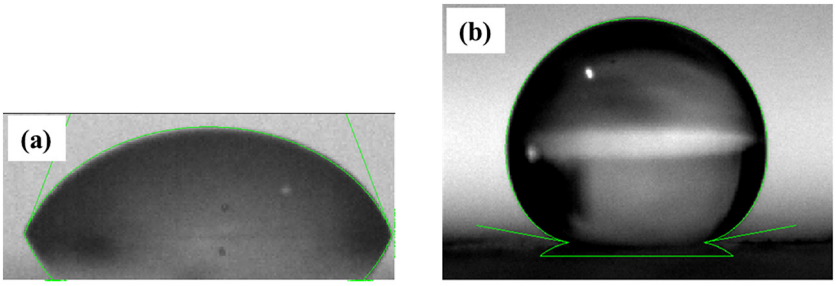

Fig. 3. Water droplets on compared surfaces: (a) hydrophilic Surface-I; (b) superhydrophobic Surface-II.

over the two compared surfaces were measured using the similar procedure as described in Waldman et al. [33]. As shown clearly in Fig. 3(a), the contact angle of the water droplet sitting on Surface-I is obviously smaller than 90° (i.e., measured $\theta \approx 65°$), demonstrating a hydrophilic surface. The measured contact angle of the water droplets on Surface-II was found to be about 157° as shown in Fig. 3(b), indicating a superhydrophobic surface (i.e., SHS in short).

By using a similar needle-in-the-sessile-drop method as that described in Korhonen et al. [40], the receding and advancing angles of water droplets (i.e., $\theta_{advancing}$ and $\theta_{receding}$) over the two compared propeller surfaces (i.e., Surface-I *vs*. Surface-II) were also measured in the present study. Table 2 summarizes the measured receding and advancing angles of the water droplets on the two studied surfaces. While the contact angle hysteresis (i.e., the difference between the advancing and receding contact angles of the water droplets, $\Delta\theta = \theta_{advancing} - \theta_{receding}$) for the hydrophilic Surface-I was found to be greater than 50°, the contact angle hysteresis for the superhydrophobic Surface-II was found to be very small, less than 5°.

It is well known that a water droplet would move over a test surface if the capillary force acting on the water droplet can be overcome by an external force (e.g., the shear force exerted by the incoming airflow on the water droplet sitting on the propeller surface for the present study). As described in Waldman et al. [33], the capillary force acting on a moving water droplet over a test plate can be estimated based on following equation:

$$F_{capillary} \approx \pi R \gamma_{LG} \left[\sin\left(\frac{\theta_{adv} - \theta_{rec}}{2}\right) \sin\left(\frac{\theta_{adv} + \theta_{rec}}{2}\right) \right] \quad (1)$$

where γ_{LG} is the liquid-gas surface tensions, and R is the spherical cap radius of the water droplet. $\theta_{advancing}$ and $\theta_{receding}$ are the advancing and receding angles of the water droplet, respectively.

Based on the measured receding and advancing angles given in Table 2, the ratio between the capillary forces acting on the water droplets with same spherical cap radii on the two compared surfaces (i.e., hydrophilic Surface-I *vs.* superhydrophobic Surface-II) can be estimated with the Eqn. (2), which can be expressed as:

$$\frac{F_{cap,\text{Surface-I}}}{F_{cap,\text{Surface-II}}} \approx \frac{[\sin(\frac{\theta_{adv}-\theta_{rec}}{2})\sin(\frac{\theta_{adv}+\theta_{rec}}{2})]_{\text{Surface-I}}}{[\sin(\frac{\theta_{adv}-\theta_{rec}}{2})\sin(\frac{\theta_{adv}+\theta_{rec}}{2})]_{\text{Surface-II}}} \approx 25 \quad (2)$$

It reveals clearly that, in comparison with those acting on water droplets on the hydrophilic Surface-I, the capillary forces acting on the water droplets with same spherical cap radius over the superhydrophobic Surface-II were found to be much smaller (i.e., 1/25th). Therefore, in order to make the water droplets to move over the superhydrophobic Surface-II, only very small external forces (i.e., only ~4% of the force magnitude) are needed to overcome the much smaller capillary forces. It also suggests that, when driven by the same incoming airflow over the propeller surface for the ice accretion experiment of the present study, the impacted water droplets/rivulets were expected to flow much faster over the superhydrophobic Surface-II, in comparison with those over the hydrophilic Surface-I.

Table 2
The measured surface properties of Surface-I and Surface-II.

Compared surface	Wettability	Static contact angle θ_{static}	Advancing contact angle $\theta_{advancing}$	Receding contact angle $\theta_{receding}$	Hysteresis $\Delta\theta = \theta_{advancing} - \theta_{receding}$	Ice Adhesion Strength (MPa)
Surface-I	Hydrophilic	~65°	~105°	~50°	>50°	1.4 ± 0.25
Surface-II	Superhydrophobic	~157°	~159°	~154°	<5°	0.37 ± 0.09

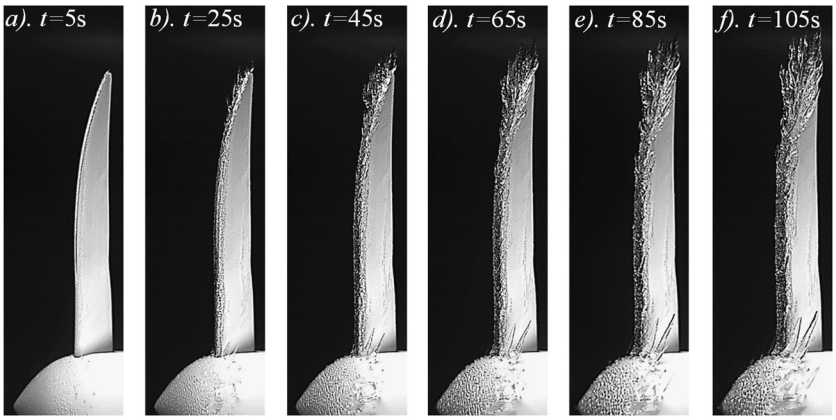

Fig. 4. Time sequences of ice accretion over the rotating propeller blade with hydrophilic Surface-I.

Using a measurement technique similar to the one described in Meuler et al. [41], the ice adhesion strengths on the two surfaces were measured and listed in Table 2 for a test plate temperature of $T_w = -10\,^{\circ}\mathrm{C}$. It can be seen clearly that, the ice adhesion strength on the superhydrophobic Surface II (i.e., ~0.37 MPa) was found to be much smaller in comparison with that on the hydrophilic surface I (i.e., ~1.4 MPa). The measured values of the ice adhesion strength on the superhydrophobic and hydrophilic surfaces were found to be in good agreement with those reported in Bharathidasan et al. [24] and Farhadi et al. [20].

3.2. Dynamic ice accretion processes over the surface of the rotating propellers with different wettability

To perform the ice accretion experiments, the ISU-IRT was operated at a pre-scribed frozen-cold temperature level (e.g., $T_\infty = -5\,^{\circ}\mathrm{C}$ for the present study) for at least 20 min under a dry airflow condition (i.e., without turning on the water spray system) to ensure that the ISU-IRT reached at a thermal steady state. After the water spray system was switched on at $t = 0$ s, supper-cooled water droplets carried by the incoming airflow impinged onto the surface of the UAS propeller model to start the ice accretion process. In the present study, with the test conditions of the freestream airflow velocity being $U_\infty = 16$ m/s, liquid water content level of $LWC = 2.0$ g/m^3, and the incoming airflow temperature of $T_\infty = -5\,^{\circ}\mathrm{C}$, the ice accretion over the surface of the rotating UAS propeller model is expected to be that of a typical glaze icing process (i.e., with obvious surface water transport and formation of transparent ice structures), as described in previous studies [39,42].

As described above, a "phase-locked" imaging technique was used to acquire "frozen" images to reveal the time evolution of the ice features accreted on the surface of the rotating propeller model. Fig. 4 shows typical "phase-locked" images for the test case with the surface of the propeller model being hydrophilic (i.e., Surface-I case). It can be seen clearly that, with super-cooled water droplets impinging onto both the rotor blades and the spinner cone, a typical glaze ice accretion process was observed, as expected. Similar to that described in Liu et al. [3], under such a wet glaze icing condition, the heat transfer process would not be fast enough to remove all the released latent heat of fusion associated with the solidification of the impinged super-cooled water droplets over the propeller surface. As a result, only a portion of the super-cooled water droplets solidified upon impact, while the remainder of the water mass stayed in liquid and flowed freely over the propeller surface. As shown clearly in Fig. 4(a) and Fig. 4(b), after the supercooled water droplets impinged onto the propeller surface, the unfrozen water mass was transported along the propeller surface in both the chordwise and spanwise directions due to the combined effects of the aerodynamic shear forces exerted by the incoming airflow and the centrifugal forces associated with the rotation motion of the propeller. As a result, in addition to the significant ice accretion along the leading edges of the rotor blades and front surface of the spinner cone (i.e., within the direct impingement zones of the incoming super-cooled water droplets), ice accretion was also found to take place further downstream away from the direct impingement zones due to the re-freezing of the runback surface water. Due to the strong effect of the centrifugal forces induced by the rotational motion, a portion of the surface water mass was found to separate from the ice accretion to form icicle structures extruding outward into the airflow, as shown clearly in Fig. 4(c). As the time goes by, with more and more super-cooled water droplets impinged onto the propeller surface, the ice accretion process over the propeller surface (i.e., on the surfaces for both rotor blades and spinner cone) was found to become very complex due to the complicated interactions among the multiphase flows (i.e., airflow, impinging water droplets, surface water transport, dynamic solidification and ice accretion, etc.…) in combination with the effects of the rotation motion. The icicle structures formed over the propeller surface were found to grow rapidly with more complex branches extruding further into the airflow. With more and more water mass impinging onto the ice accreting surface, very complex "lobster-tail-like" ice structures were found to form over the propeller surface, as shown clearly in Fig. 4(f). Such icicle features were found to cause severe wake disturbances which would significantly degrade the aerodynamic performance of the propeller [3].

After applying Hydrobead™ coating onto the surfaces of both the rotor blades and cone-shaped spinner, the propeller surfaces become superhydrophobic, characterized by a very large contact angle ($\theta \approx 157°$) and a very small contact angle hysteresis ($\Delta\theta < 5°$) for sessile water droplets sitting on the surface. Fig. 5 shows the typical snapshots of the "phase-locked" images that reveal the

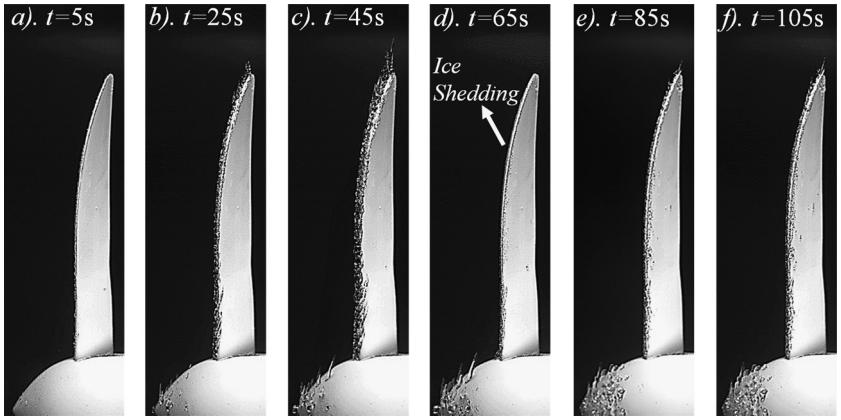

Fig. 5. Time sequences of ice accretion over the rotating propeller blade with Surface-II of SHS.

time evolution of the dynamic ice accretion process over the superhydrophobic propeller surface (i.e., Surface-II case). Based on the comparison of the acquired images given in Fig. 5 against those shown in Fig. 4, it is obvious that, owe to the unique characteristics of the superhydrophobic surface to bounce-off and to delay the freezing process of the impinged super-cooled water droplets as those reported in Li et al. [43], the ice accretion over the superhydrophobic propeller surface was found to be much less, in comparison with the test case with the propeller surface being hydrophilic (i.e., Surface-I case).

It should also be noted that, although the ice accretion over the rotating propeller surface was found to be mitigated greatly for superhydrophobic propeller, icicle structures were still found to accrete along the leading-edges of the rotor blades, as shown clearly in Fig. 5(b). This highlights one of the major technical challenges facing superhydro- and/or ice-phobic coating strategies for UAS inflight icing mitigation. As described above, while superhydrophobic coatings produce low adhesion forces between the propeller surfaces and water and/or accreted ice, and rely on aerodynamic stresses acting tangentially to the surface to remove the surface water and accreted ice, this approach would break down at the stagnation lines near the leading edges of the rotor blades because the shear stresses near the stagnation lines are very small or completely vanished. As a result, ice accretion was found to take place along the stagnation lines of the rotor blades, as shown clearly in Fig. 5. Once ice started to accrete along the stagnation lines of the rotor blades, the super-cooled water droplets carried by the incoming airflow would impact onto the surface of the accreted ice, instead of the superhydrophobic propeller surface, to cause further ice accretion. Similar phenomena were also observed by Waldman et al. [33] in their experimental study to evaluate the effects of surface wettability on the ice accretion over a fixed airfoil/wing model. With more and more super-cooled water droplets impacting and accumulating on the ice surface, the ice layers accreted along the blade leading edges were found to become thicker and thicker, as shown clearly in Fig. 5(c). Due to the strong effects of the centrifugal forces induced by the rotation motion, icicle structures were found to form along the blade leading edges for this test case. As the time goes by, the icicle structures were found to grow up to form more complex branches, extruding further into the incoming airflow to degrade the aerodynamic performance of the propeller.

As described above, the capillary forces acting on the surface water droplets/rivulets over the superhydrophobic Surface-II would be much smaller (i.e., only 1/25th in magnitude), in comparison with those over the hydrophilic Surface-I. As driven by the aerodynamic forces exerted by the same incoming airflow and the centrifugal forces induced by the same rotation motion, moving speed of the unfrozen runback water over the superhydrophobic propeller surface (i.e., Surface-II case) would be much faster, in comparison with that over the hydrophilic Surface-I case. The runback surface water was expected to roll off very quickly from the superhydrophobic propeller surface before freezing. Therefore, as shown clearly in Fig. 5, no obvious ice accretion was found in the downstream regions away from the direct impingement zones for the test case with the propeller surface becoming superhydrophobic. In comparison, in addition to the significant ice accretion along the blade leading edges, the runback water was found to be frozen into ice at further downstream regions, i.e., at the locations away from the direct impingement zones, for the test case with the propeller surface being hydrophilic, as shown clearly in Fig. 4.

With the continuous impingement and freezing of the incoming super-cooled water droplets on the propeller surface, the total mass of the ice layers accreted along the blade leading-edges would increase continuously. As described above, since the rotation speed of the propeller was kept in constant during the experiment, the centrifugal force acting on the ice layers accreted along the blade leading edges would become bigger and bigger along with the increasing total mass of the accreted ice. Once the centrifugal forces induced by the rotation motion overcome the adhesion forces of ice to the propeller surface, the ice structures were found to be completely shed off from the propeller surface, as clearly shown in Fig. 5(d). As reported quantitatively in Table 2, since the ice adhesion strength over the superhydrophobic Surface-II is much smaller than that over the hydrophilic Surface-I (i.e., 0.37 MPa of superhydrophobic Surface-II *vs.* 1.4 MPa of hydrophilic Surface-I, while the coherent strength of ice ranges from 0.7 MPa to 3.1 MPa [44]), the ice structures accreted over the superhydrophobic propeller surface (i.e., the Surface-II case) would be much easier to shed. Compared with the results given in the previous study [3], i.e., ice accretion on the bare, polished blade at the same test condition, in which a large accretion with shedding at 102 s just before the end of the test was observed, it seems that, the hydrophobic substrate would also show a benefit for ice prevention compared with the hydrophilic surface (i.e., Surface-I), though not so good as the superhydrophobic surface (i.e., Surface-II). The findings of the present study were found to agree well with those reported in the previous studies [23–26]. Following the definition described in Hejazi et al. [28], the SHS coating used in the present study can be considered as an icephobic coating due to its capability of preventing ice formation over the propeller surface and the reduced ice adhesion strength between the accreted ice layers and the propeller surface. However, the durability of superhydrophobic surfaces remains a challenge to date [45,46], which should be addressed for future development of the icephobic surfaces.

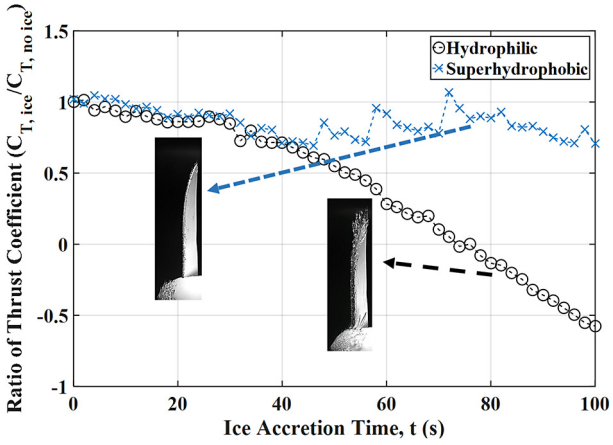

Fig. 6. Measured thrust of the propeller model with different surface wettability.

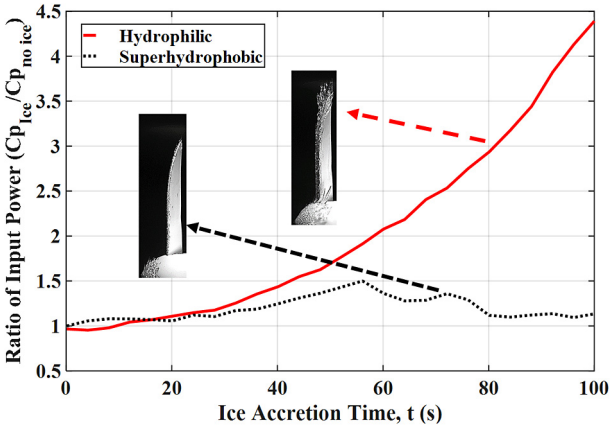

Fig. 7. Power consumption of the propeller model with different surface wettability.

3.3. Performance degradation of the propeller model due to the ice accretion

As described above, a highly sensitive JR3 load cell was used in the present study to achieve time-resolved measurements of aerodynamic loads acting on propeller models with different surface wettability (i.e., Surface-I *vs.* Surface-II) in order to evaluate the effects of the surface wettability on the propeller performance. While similar features can also be revealed by other components of the measured aerodynamic forces and moments, only the measured thrust force data is given in the present study for analysis for conciseness. Fig. 6 shows a comparison of the normalized thrust coefficients of the propeller model (normalized by the case without any ice accretion on the propeller surface). Following the work of Brandt and Selig [47], the thrust coefficient, C_T, of the propeller is defined using following equation:

$$C_T = \frac{T}{\rho n^2 D^4} \tag{3}$$

where n is rotational speed of the propeller, D is the diameter of the propeller, ρ is the air density, and T is thrust force generated by the propeller.

As described above, after the super-cooled water droplets impinged onto the rotating propeller surface, surface water transport and formation of irregular icicle accretion were observed for the test case with the propeller surface being hydrophilic (i.e., Surface-I case). The icicle structures accreted along the rotor blades dramatically distort the streamlined profiles of the propeller blades, causing significant degradation to the aerodynamic performance of the propeller (i.e., lift decrease and drag increase). As a result, the thrust generated by the propeller model with the hydrophilic surface (i.e., Surface-I case) was found to decrease rapidly, as shown clearly in Fig. 6. With more and more super-cooled water droplets impinging onto the propeller surface and producing more and more complicated "lobster-tail-like" icicle structures, the thrust coefficient was found to become negative at about 70 s after starting the ice accretion experiment, indicating a complete loss of the thrust generation capability for the propeller model. It suggests that, due to the severe ice accretion over the propeller surface, the propeller model was found actually to operate in "drag generation mode" to cause dramatic drag increase, i.e., to slow down the flying speed of the UAS, instead of "thrust generation mode" to propel the UAS flying forward.

For the test case with the propeller surface being superhydrophobic (i.e., Surface-II case), as shown in Fig. 6, a similar trend of thrust reduction was also found at the beginning of the ice accretion experiment (i.e., $t \leq 45$ s), due to the ice accretion along the stagnation lines of the rotor blades. As described above, as the mass of the ice accreted along the stagnation line near a blade leading edge increased, the centrifugal force exerted on the accreted ice structures also increased. Once the centrifugal force became greater than the interfacial adhesion force between the accreted ice and the propeller surface, the accreted ice structures would be shed off from the rotor blades, resulting in recovery of the decreased thrust coefficient, e.g., at the time instance of $t = 55$ s as shown in Fig. 6. With multiple cycles of the ice accretion and shed-off, the thrust coefficient of the propeller model with the superhydrophobic surface (i.e., Surface-II case) was found always to remain in "thrust generation mode" with the normalized thrust coefficient being greater than 80% for the rest of the experiment, which is significantly different from the test case with the hydrophilic surface (Surface-I) that operated in "drag generation mode" due to the severe ice accretion over the propeller surface.

As described above, while the propeller model was operated at a constant rotation speed of $n = 3{,}000$ rpm during the ice accretion experiment, the needed power inputs (i.e., power consumption) to drive the propeller model (i.e., Surface-I *vs.* Surface-II) were also monitored for comparison. Fig. 7 shows the time evolution of the required power inputs for the propeller model during the dynamic icing process. Following the work of Brandt and Selig [47], the power consumption coefficient, C_P, of the propeller is defined as:

$$C_P = \frac{P}{\rho n^3 D^5} \tag{4}$$

In order to reveal the effects of ice accretion on the power consumption characteristics of the propeller models more clearly, the power inputs required to drive the propeller models during the ice accretion experiment were normalized by the power required to drive the propeller model with no ice, i.e., before switching on the spray system to start the ice accretion process. As revealed clearly in Fig. 7, for the test case with the propeller surface being hydrophilic (i.e., Surface-I case), the required power input was found to increase dramatically and monotonically during the ice accretion experiment. It can be explained by the fact that, very complex icicle structures were generated on both the rotating propeller blades and the propeller spinner (e.g., the formation of complex "lobster-tail-like" structures) for this test case, as shown clearly in Fig. 4. Since the shapes of the accreted ice structures over the propeller surfaces were highly irregular, they would drastically degrade the aerodynamic performance of the propeller model. As a result, the aerodynamic drag acting on the propeller and the total mass of the iced propeller would increase significantly. Therefore, a much greater power input was required in order to keep the propeller rotating at the same rotation speed (i.e., up to about 330% more

power input is required at about 100 s after starting the ice accretion process), as shown in Fig. 7.

For the test case with the propeller surface being superhydrophobic (i.e., Surface-II case), corresponding to the ice accretion along the stagnation lines of the propeller blades to degrade the aerodynamic performance of the propeller as described above, the required power inputs for this test case were also found to increase monotonically at the beginning of the ice accretion experiment (i.e., $t < 50$ s). The required power input due to the ice accretion for the propeller was found to increase ~40% at about 50 s after starting the ice accretion experiment. It can also be seen that, corresponding to the shedding of the accreted ice structures from the superhydrophobic propeller surface at the time instance of $t \approx 55$ as shown in Fig. 7, the required power inputs for the propeller model was found to decrease gradually, due to the recovery of the propeller aerodynamic performance associated with the ice shed-off. With multiple ice accretion and shedding cycles taking place over the superhydrophobic propeller surface, the required power inputs for the propeller model were found to fluctuate up and down during the ice accretion experiment, as expected.

However, in comparison with those with the propeller surface being hydrophilic (i.e., Surface-I case), the required power inputs for this test case with the propeller surface being superhydrophobic (i.e., Surface-II case) were found to be significantly reduced during the ice accretion experiment, due to the much less ice accretion over the propeller surface as shown in Fig. 5. It indicates that the excess power consumption due to ice accretion would be significantly reduced by making the propeller surface superhydrophobic (i.e., over ~75% less power input after 100 s of ice accretion). The much less power consumption of the UAS propeller in the icing conditions would indicate a much longer flight duration for the UAS operation in cold weathers.

4. Conclusion

An experimental study was conducted to examine the effects of surface wettability on the dynamic ice accretion process over the surface of a rotating UAS propeller model and the resultant performance degradation due to the ice accretion. The experimental study was conducted in an Icing Research Tunnel available at Iowa State University (i.e., ISU-IRT) with a typical UAS propeller model operated under a typical glaze icing condition. During the experiment, the surface of UAS propeller model was treated to change its surface wettability (i.e., hydrophilic surface case *versus* superhydrophobic surface case). While a high-speed imaging system was used to acquire "phase-locked" images to reveal the dynamic ice accretion process over the rotating propeller surface, the thrust force generated by the propeller model and the required power inputs to drive the propeller model to operate at a constant rotation speed were also measured simultaneously during the ice accretion experiment.

With the ISU-IRT operating in an icing condition with relatively low incoming airflow velocity of $U_\infty = 16$ m/s, relatively warm ambient temperature of $T_\infty = -5\,^\circ$C; and a relatively high Liquid Water Content (*LWC*) level of 2.0 g/m^3, the ice accretion over the surface of the rotating propeller model was found to be of a typical *glaze* ice accretion process, as expected. While only a portion of the incoming super-cooled water droplets froze upon impact, the rest of the impinged water mass was in a liquid state and could flow freely over the propeller surface. For the test case with the propeller surface being hydrophilic (i.e., Surface-I case), the combined effects of the aerodynamic shear force exerted by the incoming airflow and the centrifugal force associated with the rotational motion produced a very complex glaze ice accretion. The unfrozen water mass was found to run back along the hydrophilic surface and eventually froze resulting in the formation of very complex icicles or even "lobster-tail-like" ice structures. Such glaze ice accretion was found to degrade the aerodynamic performance of the propeller model significantly. Correlated with the increase of accreted ice over time, the thrust was observed to decrease rapidly while the power required to drive the propeller model increased dramatically. With the formation of more and more complicated "lobster-tail-liked" icicle structures over surfaces of the propeller blades, the iced propeller model was found to operate in "drag generation mode", instead of "thrust generation mode", to cause significant drag to slow down the flying speed of the UAS, instead of generating thrust to propel the UAS flying forward. It was also found that, in comparison with the baseline case without any ice accretion on the propeller surface, up to 330% more power input was required to drive the iced propeller model at about 100 s after starting the glaze ice accretion experiment for the test case with the propeller surface being hydrophilic (i.e., Surface-I case).

However, for the test case with the propeller surface being superhydrophobic (i.e., the Surface-II case), while ice accretion was still found to take place along the stagnation lines of the rotor blades, the total amount of the ice accreted over the superhydrophobic propeller surface were found to become significantly less, in comparison with those with the propeller surface being hydrophilic (i.e., the Surface-I case). Due to the much smaller capillary forces over the superhydrophobic surface, the surface water was found to run back much faster over the superhydrophobic propeller surface, in comparison with those over the hydrophilic propeller surface. As a result, the runback surface water was found to roll-off very quickly from the superhydrophobic propeller surface before being frozen into ice. As a result, no obvious ice accretion was found at further downstream regions away from the direct impingement zones of the water droplets. With the much smaller ice adhesion strength over the superhydrophobic surface, the ice structures accreted over the superhydrophobic propeller surface were also found to be much easier to shed, in comparison with those accreted over the hydrophilic propeller surface (i.e., the Surface-I case). As the accreted ice structures were shed from the superhydrophobic propeller surface, the thrust of the propeller model was found to recover gradually. With multiple cycles of ice accretion and shedding, the propeller model with superhydrophobic surface (i.e., Surface-II case) was found to always remain in "thrust generation mode" during the glaze ice accretion experiment.

In summary, the dynamic ice accretion process and the resultant aerodynamic performance of the UAS propeller were found to be affected greatly by the surface wettability of the propeller model. By treating the propeller surface with a superhydrophobic coating, the detrimental effects of ice accretion on the aerodynamic performance of the propeller model were mitigated greatly relative to the results for the hydrophilic propeller, as indicated by much less ice accretion on the propeller surface, a reduction of the thrust loss (~70% less) and a reduction in power consumption (~75% less) during the glaze ice accretion experiment. The great reduction in the thrust loss and the power consumption for the UAS propellers would promise safer and longer flight duration for UAS operations under icing conditions.

Conflict of interest statement

There is no conflict of interest.

Acknowledgements

The authors want to thank Dr. Rye Waldman, Mr. Prashanth Sagar, Mr. James Benson and Mr. Andrew Jordan of Iowa State University for their help in operating ISU Icing Research Tunnel (ISU-IRT) Facility. The research work is partially supported by

Iowa Space Grant Consortium (ISGC) Base Program for Aircraft Icing Studies, National Aeronautics and Space Administration (NASA) with the grant numbers of NNX16AN21A and NNX12C21A, and National Science Foundation (NSF) under award numbers of CBET-1064196 and CBET-1435590.

References

[1] M.B. Bragg, A.P. Broeren, L.A. Blumenthal, Iced-airfoil aerodynamics, Prog. Aerosp. Sci. 41 (5) (2005) 323–362, https://doi.org/10.1016/j.paerosci.2005.07.001.
[2] S.F. Armanini, M. Polak, J.E. Gautrey, A. Lucas, J.F. Whidborne, Decision-making for unmanned aerial vehicle operation in icing conditions, CEAS Aeronaut. J. 7 (4) (2016) 663–675, https://doi.org/10.1007/s13272-016-0215-2.
[3] Y. Liu, L. Li, Z. Ning, H. Hu, An Experimental Study on the Transient Ice Accretion Process over a Rotating UAV Propeller, AIAA Paper 2017-0727, 2017, https://doi.org/10.2514/6.2017-0727.
[4] P. Tran, G. Baruzzi, F. Tremblay, P. Benquet, FENSAP-ICE Applications to Unmanned Aerial Vehicles (UAV), AIAA Paper 2004-0402, 2004, https://doi.org/10.2514/6.2004-402.
[5] G. Botura, A. Fahrner, Icing Detection System – Conception, Development, Testing and Applicability to UAVs, AIAA Paper 2003-6637, 2003, https://doi.org/10.2514/6.2003-6637.
[6] K. Szilder, S. McIlwain, In-flight icing of UAVs – the influence of flight speed coupled with chord size, Can. Aeronaut. Space J. 58 (2) (2012) 83–94, https://doi.org/10.5589/q12-007.
[7] B. Zhang, L. Tang, M. Roemer, Probabilistic weather forecasting analysis for unmanned aerial vehicle path planning, J. Guid. Control Dyn. 37 (1) (2014) 309–312, https://doi.org/10.2514/1.61651.
[8] S.K. Thomas, R.P. Cassoni, C.D. MacArthur, Aircraft anti-icing and de-icing techniques and modeling, J. Aircr. 33 (5) (1996) 841–854, https://doi.org/10.2514/3.47027.
[9] L. Cao, A.K. Jones, V.K. Sikka, J. Wu, D. Gao, Anti-icing superhydrophobic coatings, Langmuir, ACS J. Surf. Colloids 25 (21) (2009) 12444–12448, https://doi.org/10.1021/la902882b.
[10] J. Lv, Y. Song, L. Jiang, J. Wang, Bio-inspired strategies for anti-icing, ACS Nano 8 (4) (2014) 3152–3169, https://doi.org/10.1021/nn406522n.
[11] Y. Liu, L.J. Bond, H. Hu, Ultrasonic-attenuation-based technique for ice characterization pertinent to aircraft icing phenomena, AIAA J. 55 (5) (2017) 1602–1609, https://doi.org/10.2514/1.J055500.
[12] O. Parent, A. Ilinca, Anti-icing and de-icing techniques for wind turbines: critical review, Cold Reg. Sci. Technol. 65 (1) (2011) 88–96, https://doi.org/10.1016/j.coldregions.2010.01.005.
[13] Y. Cheng, D. Rodak, C. Wong, C. Hayden, Effects of micro- and nano-structures on the self-cleaning behaviour of lotus leaves, Nanotechnology 17 (5) (2006) 1359–1362, https://doi.org/10.1088/0957-4484/17/5/032.
[14] Y. Liu, X. Chen, J. Xin, Hydrophobic duck feathers and their simulation on textile substrates for water repellent treatment, Bioinspir. Biomim. 3 (4) (2008) 046007, https://doi.org/10.1088/1748-3182/3/4/046007.
[15] K. Koch, B. Bhushan, Y. Jung, W. Barthlott, Fabrication of artificial lotus leaves and significance of hierarchical structure for superhydrophobicity and low adhesion, Soft Matter 5 (2009) 1386–1393, https://doi.org/10.1039/B818940D.
[16] S. Wang, K. Liu, X. Yao, L. Jiang, Bioinspired surfaces with superwettability: new insight on theory, design, and applications, Chem. Rev. 115 (16) (2015) 8230–8293, https://doi.org/10.1021/cr400083y.
[17] Z. Guo, W. Liu, B.-L. Su, Superhydrophobic surfaces: from natural to biomimetic to functional, J. Colloid Interface Sci. 353 (2) (2011) 335–355, https://doi.org/10.1016/j.jcis.2010.08.047.
[18] Y.H. Yeong, R. Mudafort, A. Steele, I. Bayer, E. Loth, G. De Combarieu, Water Droplet Impact Dynamics at Icing Conditions with and Without Superhydrophobicity, AIAA Paper 2012-3134, 2012, https://doi.org/10.2514/6.2012-3134.
[19] H.K. Webb, R.J. Crawford, E.P. Ivanova, Wettability of natural superhydrophobic surfaces, Adv. Colloid Interface Sci. 210 (2014) 58–64, https://doi.org/10.1016/j.cis.2014.01.020.
[20] S. Farhadi, M. Farzaneh, S.A. Kulinich, Anti-icing performance of superhydrophobic surfaces, Appl. Surf. Sci. 257 (14) (2011) 6264–6269, https://doi.org/10.1016/j.apsusc.2011.02.057.
[21] L. Oberli, D. Caruso, C. Hall, M. Fabretto, P.J. Murphy, D. Evans, Condensation and freezing of droplets on superhydrophobic surfaces, Adv. Colloid Interface Sci. 210 (2014) 47–57, https://doi.org/10.1016/j.cis.2013.10.018.
[22] C. Antonini, M. Innocenti, T. Horn, M. Marengo, A. Amirfazli, Understanding the effect of superhydrophobic coatings on energy reduction in anti-icing systems, Cold Reg. Sci. Technol. 67 (1–2) (2011) 58–67, https://doi.org/10.1016/j.coldregions.2011.02.006.
[23] H. Zhu, Z. Guo, W. Liu, Adhesion behaviors on superhydrophobic surfaces, Chem. Commun. 50 (2014) 3900–3913, https://doi.org/10.1039/c3cc47818a.
[24] T. Bharathidasan, S.V. Kumar, M.S. Bobji, R.P.S. Chakradhar, B.J. Basu, Effect of wettability and surface roughness on ice-adhesion strength of hydrophilic, hydrophobic and superhydrophobic surfaces, Appl. Surf. Sci. 314 (2014) 241–250, https://doi.org/10.1016/j.apsusc.2014.06.101.
[25] M.A. Sarshar, C. Swarctz, S. Hunter, J. Simpson, C.-H. Choi, Effects of contact angle hysteresis on ice adhesion and growth on superhydrophobic surfaces under dynamic flow conditions, Colloid Polym. Sci. 291 (2) (2013) 427–435, https://doi.org/10.1007/s00396-012-2753-4.
[26] S.A. Kulinich, M. Farzaneh, Ice adhesion on super-hydrophobic surfaces, Appl. Surf. Sci. 255 (2009) 8153–8157, https://doi.org/10.1016/j.apsusc.2009.05.033.
[27] S. Jung, M. Dorrestijn, D. Raps, A. Das, C.M. Megaridis, D. Poulikakos, Are superhydrophobic surfaces best for icephobicity?, Langmuir 27 (6) (2011) 3059–3066, https://doi.org/10.1021/la104762g.
[28] V. Hejazi, K. Sobolev, M. Nosonovsky, P.K. Rohatgi, From superhydrophobicity to icephobicity: forces and interaction analysis, Sci. Rep. 3 (2013) 70–71, https://doi.org/10.1038/srep02194.
[29] J. Chen, J. Liu, M. He, K. Li, D. Cui, Q. Zhang, X. Zeng, Y. Zhang, J. Wang, Y. Song, Superhydrophobic surfaces cannot reduce ice adhesion, Appl. Phys. Lett. 101 (2012) 111603, https://doi.org/10.1063/1.4752436.
[30] M. Nosonovsky, V. Hejazi, Why superhydrophobic surfaces are not always icephobic, ACS Nano 6 (10) (2012) 8488–8491, https://doi.org/10.1021/nn302138r.
[31] K. Varanasi, T. Deng, J. Smith, Frost formation and ice adhesion on superhydrophobic surfaces, Appl. Phys. Lett. 97 (2010) 8234102, https://doi.org/10.1063/1.3524513.
[32] T. Maitra, M.K. Tiwari, C. Antonini, P. Schoch, S. Jung, P. Eberle, D. Poulikakos, On the nanoengineering of superhydrophobic and impalement resistant surface textures below the freezing temperature, Nano Lett. 14 (2014) 172–182, https://doi.org/10.1021/nl4037092.
[33] R.M. Waldman, H. Li, H. Hu, An Experimental Investigation on the Effects of Surface Wettability on Water Runback and Ice Accretion over an Airfoil Surface, AIAA Paper 2016-3139, 2016, https://doi.org/10.2514/6.2016-3139.
[34] A. Marmur, Wetting on hydrophobic rough surfaces: to be heterogeneous or not to be?, Langmuir. 19 (2003) 8343–8348, https://doi.org/10.1021/la0344682.
[35] H. Vahabi, W. Wang, K.C. Popat, G. Kwon, T.B. Holland, A.K. Kota, Metallic superhydrophobic surfaces via thermal sensitization, Appl. Phys. Lett. 110 (2017) 251602, https://doi.org/10.1063/1.4989577.
[36] W. Wang, J. Salazar, H. Vahabi, A. Joshi-Imre, W.E. Voit, A.K. Kota, Metamorphic superomniphobic surfaces, Adv. Mater. 29 (2017) 1700295, https://doi.org/10.1002/adma.201700295.
[37] Y. Wang, J. Xue, Q. Wang, Q. Chen, J. Ding, Verification of icephobic/anti-icing properties of a superhydrophobic surface, ACS Appl. Mater. Interfaces 5 (8) (2013) 3370–3381, https://doi.org/10.1021/am400429q.
[38] X. Sun, V.G. Damle, S. Liu, K. Rykaczewski, Bioinspired stimuli-responsive and antifreeze-secreting anti-icing coatings, Adv. Mater. Interfaces 2 (2015) 1400479, https://doi.org/10.1002/admi.201400479.
[39] R.M. Waldman, H. Hu, High-speed imaging to quantify transient ice accretion process over an airfoil, J. Aircr. 53 (2) (2015) 369–377, https://doi.org/10.2514/1.C033367.
[40] J.T. Korhonen, T. Huhtamäki, O. Ikkala, R.H.A. Ras, Reliable measurement of the receding contact angle, Langmuir 29 (2013) 3858–3863, https://doi.org/10.1021/la400009m.
[41] A.J. Meuler, J.D. Smith, K.K. Varanasi, J.M. Mabry, G.H. McKinley, R.E. Cohen, Relationships between water wettability and ice adhesion, ACS Appl. Mater. Interfaces 2 (2010) 3100–3110, https://doi.org/10.1021/am1006035.
[42] R.J. Hansman, M.S. Kirby, Comparison of wet and dry growth in artificial and flight icing conditions, J. Thermophys. Heat Transf. 1 (3) (1987) 215–221, https://doi.org/10.2514/3.30.
[43] H. Li, R.M. Waldman, H. Hu, An Experimental Investigation on Unsteady Heat Transfer and Transient Icing Process upon Impingement of Water Droplets, AIAA Paper 2016-0510, 2016, https://doi.org/10.2514/6.2016-0510.
[44] J.J. Petrovic, Review Mechanical properties of ice and snow, J. Mater. Sci. 38 (2003) 1–6, https://doi.org/10.1023/A:1021134128038.
[45] X. Tian, T. Verho, R.H.A. Ras, Moving superhydrophobic surfaces toward real-world applications, Science 352 (6282) (2016) 142–143, https://doi.org/10.1126/science.aaf2073.
[46] W. Wang, K. Lockwood, L. Boyd, Superhydrophobic coatings with edible materials, ACS Appl. Mater. Interfaces 8 (2016) 18664–18668, https://doi.org/10.1021/acsami.6b06958.
[47] J. Brandt, M. Selig, Propeller Performance Data at Low Reynolds Numbers, AIAA Paper 2011-1255, 2011, https://doi.org/10.2514/6.2011-1255.